Highly microcrystalline phosphorous-doped Si:H very thin films deposited by RF-PECVD

Alestair Wilson, Erwann Fourmond, Bilel Saidi, Benjamin Fornacciari, Solène Brottet, Marc Juhel, Mickael Gros-Jean

Highly microcrystalline phosphorous-doped Si:H very thin films deposited by RF-PECVD

Alestair Wilson, Erwann Fourmond, Bilel Saidi, Benjamin Fornacciari, Solène Brottet, Marc Juhel, and Mickael Gros-Jean*

A. Wilson, B. Saidi, M. Juhel, M. Gros-Jean
STMicroelectronics, 850 rue Jean Monnet, 38926 Crolles, France
E-mail : alestair.wilson@insa-lyon.fr

A. Wilson, E. Fourmond, B. Fornacciari, S. Brottet
Univ Lyon, INSA Lyon, CNRS, Ecole Centrale de Lyon, Université Claude Bernard Lyon 1, CPE Lyon, INL, UMR5270, 69621 Villeurbanne, France

Keywords: Hydrogenated, Microcrystalline, Silicon, Phosphorus, Doping, Above-IC, Image Sensor

Abstract

Finely tuning crystallinity and doping of hydrogenated microcristalline silicon thin films is a keypoint into obtaining high quality devices for above integrated circuit (above-IC) image sensors. This study focuses on the structural and electrical properties of RF-PECVD deposited microcrystalline silicon (µc-Si:H) contact layers. In this work, phosphorus doped µc-Si:H is deposited by capacitive coupled plasma RF-PECVD (13,56 MHz) from a SiH_4 + H_2 + PH_3 gas mixture with varying phosphine concentration. The influence of phosphine concentration on dopant concentration, active dopant concentration and crystallinity is studied by SIMS, Hall effect measurement and Raman spectroscopy respectively. High doping level is attained, reaching up to 1.7×10^{20} cm^{-3}. Furthermore, “low power” and “high power” deposition conditions are studied which lead to incubation layers of different nature.

1. Introduction

CMOS image sensors have now replaced CCD sensors in a vast majority of applications due to their better performance in energy consumption and speed as well as their compatibility with standard CMOS integrated circuit.[1], [2] Amongst CMOS sensors the two most common architectures, i.e., frontside illuminated sensors and backside illuminated sensors, have well known

downsides such as shading from metallic interconnection and additional costs due to integration complexity,[3] respectively. A proposed alternative has been to introduce above-IC image sensors,[4] which tacle the forementionned issues by placing the light sensitive region above the integrated circuit. Such a design comes with strong constraints on the process temperature allowed to produce the photodiode since copper diffusion can occur above 350 °C, leading to critical midgap defects in silicon based transistors.[5]

Some strong candidates for such purpose are Silicon and Germanium-based semiconductor materials which can be deposited in their amorphous or microcrystalline phase by PECVD at temperatures well under 350 °C. [6]–[8] Our work will focus on exploring the growth process as well as the structural and electrical properties of n-type (P-doped) µc-Si:H. Undoped µc-Si:H deposited by PECVD typically exhibits an amorphous incubation layer which can span up to 100 nm before nucleation of the crystalline phase.[9] Previous work conducted by other research groups on SiGe-based P-I-N sensors have shown that the n and p type layers typically have a thickness of the order of a few tens of nanometers.[10], [11] It is thus of great interest to understand the structural nature of thin layers as well as the impact of phosphorus doping on their properties.

In this work we have studied the impact of deposition process parameters for micro-crystalline silicon phosphorous-doped layers, such as power, pressure and hydrogen dilution on film properties. Crystalline volume fraction, active and absolute dopant concentration as well as incubation layer thickness were measured and deposition conditions were found which gave a high doping level as well as a thin incubation layer.

2. Experimental Section

Films were deposited using a capacitively coupled PECVD setup working at 13,56 MHz. The showerhead-type powered electrode as well as the anode are 300 mm in diameter. The anode is at floating potential due to the reactor's design. All the films were deposited at a temperature of 250 °C, on both glass (soda lime) and monocrystalline silicon. The glass substrates were cleaned using ultrasonic bath in an ethanol solution at 40 °C and rinced with deionized (DI) water while silicon was deoxydized in a 5% HF solution before being rinced with DI water. Deposition pressure was varied between 800 and 1000 mTorr and power set at 30 or 100 W. Gases used for deposition include pure silane (SiH_4), pure hydrogen (H_2) and hydrogen-diluted phosphine (0.1 % PH_3 in H_2). We define the hydrogen dilution factor $R_H = \phi_{H2}/\phi_{SiH4}$ and the dopant gas ratio $\beta = \phi_{PH3}/\phi_{SiH4}$ where ϕ_{PH3} is the pure (undiluted) phosphine gas flow in

sccm. Geometrical parameters such as film thickness or roughness were measured by SEM (TESCAN) and AFM (Brucker).

The crystalline volume fraction of our films was estimated locally by Raman spectroscopy using a 473 nm laser excitation. At such wavelength the absorption coefficient in both a-Si:H and µc-Si:H is low enough to ensure the incident photons reach the entire depth of the films, thus providing an averaged value for crystallinity over the whole film thickness. The transverse optical component (TO) of the spectrum obtained is then smoothed and deconvoluted into three gaussian components as reported elsewhere in the litterature[12]–[15]: an amorphous phase contribution centered around 480 cm^{-1}, grain boundaries contribution centered around 500 cm^{-1} and a crystalline phase peak centered around 521 cm^{-1}.[12] The Raman cristallinity X_c is then obtained from the following formula :

$$X_c = \frac{I_c + I_{gb}}{I_c + I_{gb} + \gamma \cdot I_a}$$

Where I_c, I_{gb} and I_a are the areas of the crystalline, grain boundary and amorphous gaussians, respectively. Factor γ is a correction factor for the difference in scattering cross-section of amorphous and crystalline Silicon given by Bustarret et al.[14] From the area of these gaussians information on the crystallinity can be obtained, called the Raman cristallinity X_c. Analysis were performed on glass-deposited films to avoid any contribution of mono-Si substrate to the spectrum which would lead to an overestimation of X_c. The absolute concentration in phosphorus atoms in our films was estimated by Time-of-Flight Secondary Ion Mass Spectrometry (ToF-SIMS) measurements (Cs^+ 2keV beam). Charge carrier concentration n and hence active dopant concentration was measured by Hall effect (Van der Pauw configuration) at room temperature. Electrical contacts for Hall measurements were done using liquid InGa alloy and ohmic behaviour of the contacts in the range 0 – 10 V was tested prior to measurement.

3. Results & Discussion

3.1. Structural properties

3.1.1. n-type doping impact on structural properties

Phosphorus doped µc-Si:H films with varying doping gas ratio β between 0 and 1% were deposited in order to investigate the impact of n-type dopant incorporation on the crystalline volume fraction obtained by raman spectrometry as shown in **Erreur ! Source du renvoi introuvable. (a)**. Erreur ! Source du renvoi introuvable. **(b)** represents the calculated Raman crystallinity X_c as a function of β for different deposition conditions. By setting the hydrogen dilution

ratio R_H at 25, power at 30 W, pressure at 800 mTorr and $t_{deposition}$ = 40 min, undoped films reach a Raman crystallinity level of 55% yet adding phosphine to the gas mixture causes a drop in X_c until the film is purely amorphous ($\beta \geq 0.5$ %). Similar influence on the formation of a crystalline phase has been reported by Guo and Gueng[10] in the case of boron dopant incoporation. In our case, this issue was tacled by working with two deposition conditions, "low power" and "high power", for both of which R_H was increased to 50. The corresponding deposition parameters can be found in **Table 1**.

Table 1 : Deposition conditions for P doped µc-Si:H

	Temperature [°C]	Pressure [mTorr]	Power [W]	Power density [mW.cm^{-2}]	$t_{deposition}$ [min]	Thickness [nm]	β	R_H
R_H 25	250	800	30	42	40	160	0% to 1%	25
Low power	250	800	30	42	60	168	0% to 1%	50
High power	250	1000	100	142	60	310	0% to 1%	50

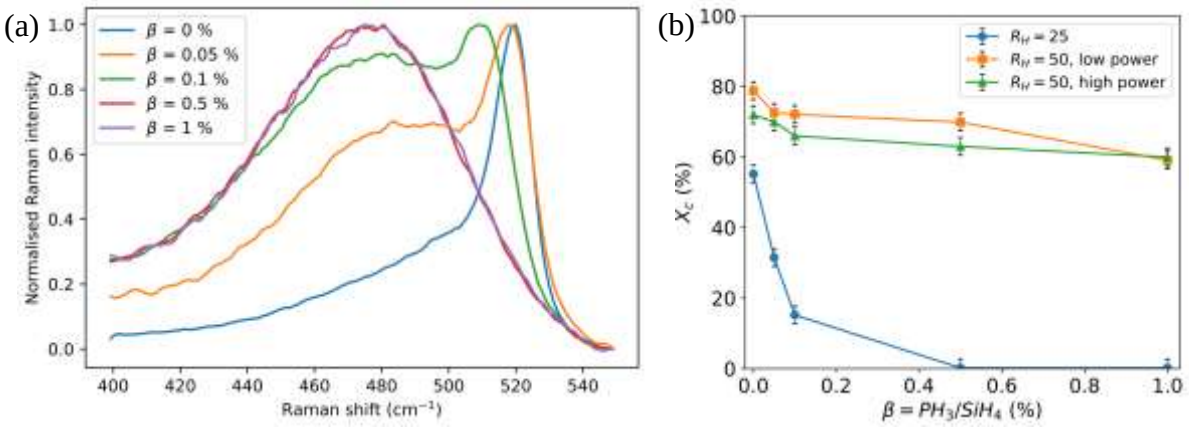

Figure 1: (a) Raman spectra of samples deposited using R_H = 25 for different gas phase concentration of phosphine β. The redshift and broadening of the Si-Si peak shows the crystalline to amorphous transition (b) Dependence of Raman crystallinity X_c on doping level in different deposition conditions, film thickness for R_H = 25, low power and high power samples are 160 nm, 168 nm and 310 nm respectively.

In undoped µc-Si:H, increase in R_H is known to impact strongly X_c until a sharp transition from amorphous to crystalline phase occurs,[16], [17] usually for R_H > 20 in our conditions. High compressive stress was observed in P doped µc-Si:H by Wei et al.[18] in similar experimental conditions. This leads us to formulate the hypothesis that the phase transition has a mechanical origin, as phosphorus may prevent the nucleation of crystalline domains, their size (typically in

the range of 10 to 20 nm) being unable accommodate the lattice deformation induced by tetravalent P atoms. A greater amount of energy is needed to allow the material to transition from a metastable amorphous phase to a crystalline one. Increasing R_H is a way to provide energy locally without a need for annealing or high temperature processes. In our experiment we were able to maintain $X_c > 60$ % in the whole range tested. The slow but continuous drop in X_c as β increases for both low and high power films supports the idea that increasing phosphorus concentration while providing a constant amount of energy (or R_H) necessarily leads to an increasing amount of amorphous phase in our layers.

3.1.2. Incubation layer growth

While in doped samples, low and high power deposition conditions lead to negligible change in X_c at constant β, a strong difference in deposition rates due to the difference in applied power between low power (2.7 nm.min^{-1}) and high power (5.2 nm.min^{-1}) films was noticed. The deposition rate was unaffected by the doping gas ratio. Incubation layer thickness in both these conditions was studied by depositing 6 layers of increasing thickness on glass substrates while keeping β constant at 0.1%. The impact of doped layer thickness on X_c is shown in **Figure 2 (a)**. Layer thickness was estimated based on the deposition rate obtained via SEM images on thicker samples. Our measurements show a sharp transition from amorphous to crystalline phase when the low power layer exceeds 35 nm. In high power conditions however crystalline phase is detected in small amounts even for the thinnest layer and increases steadily with film thickness.

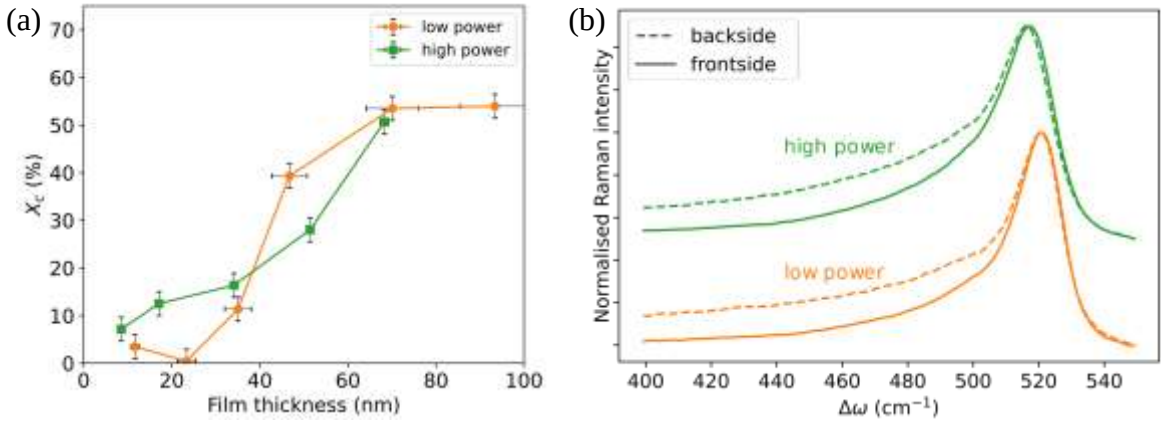

Figure 2: (a) Dependence of Raman crystallinity X_c on deposited film thickness for $\beta = 0.1\%$ (b) Frontside and backside Raman spectra of low and high power deposited films. The noticeable increase in signal intensity in the amorphous region (480 cm^{-1}) reveals the presence of an amorphous phase at the interface with the substrate.

In order to verify the region near the substrate remained amorphous even when increasing the thickness of the film Raman spectra were measured on both the frontside and backside of the thicker films. The backside measurements were taken through the glass substrate and its contribution to the spectrum was corrected by substracting the spectrum of a pristine glass substrate. The optical scattering depth at the excitation wavelength (λ_{exc} = 473 nm) is of the order of α^{-1}, i.e., 35 nm for a-Si:H and 160 nm for µc-Si:H. Probing of the layer through Raman scattering is thus sensitive to the chosen side for optical excitation. **Figure 2 (b)** shows the normalised Raman spectra in both cases, for the low power and high power $\beta = 0.1\%$ samples (168 nm and 310 nm respectively). The broadening of the spectrum towards the amorphous region (~ 480 cm^{-1}) supports the existence of an amorphous phase located close to the substrate/film interface. For the low power sample, calculation of X_c yields a value of 67 % from the frontside and 55 % from the backside, while the high power sample yields X_c = 72 % and 57 % from the frontside and backside, respectively. Although Raman spectrocopy does not provide an estimation of the incubation layer thickness, it supports the model of a thin amorphous layer at the film/substrate interface.

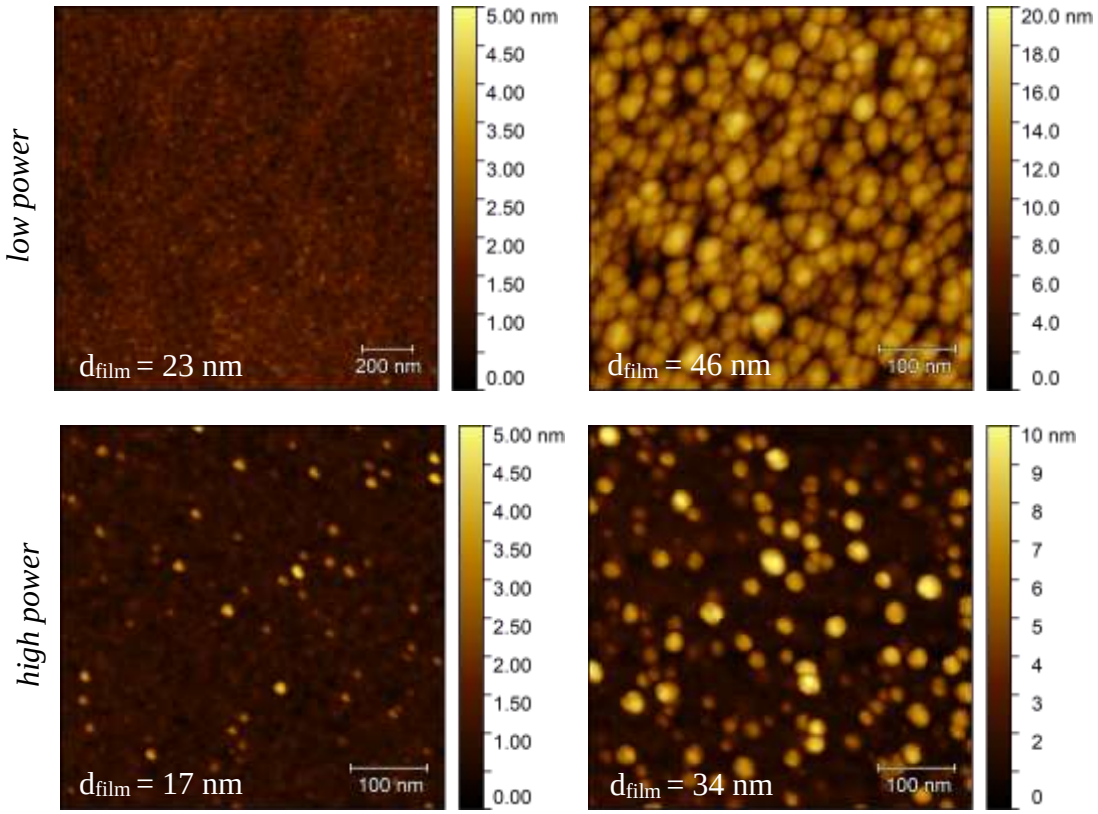

Figure 3: AFM surface image of low power (top) and high power (bottom) deposited films for two samples of increasing film thickness.

Further results were obtained by AFM measurement of the same films, deposited on mono-Si (Erreur ! Source du renvoi introuvable.). While a-Si:H deposition leads to films with little roughness as shown by Collins et al. and Abelson et al., µc-Si:H growth is in part recogniseable due to its "caufliflower-like" surface topography which emerges from the growth of the crystalline phase. This marked increase in roughness due to the presence of a crystalline phase has been described by Vallat-Sauvain et al.[19] and Matsuda[16] in hydrogenated microcrystalline Silicon and Jordan et al.[20] in hydrogenated microcrystalline Germanium thin films. In low power conditions crystalline nodules totally cover the surface in the 46 nm thin sample while the 26 nm layer shows no sign of crystalline phase. Such a change in surface topology supports our Raman spectroscopy observations regarding the sharpness of the amorphous to crystalline transition (Figure 2**Erreur ! Source du renvoi introuvable.** (a)). In high power conditions AFM imaging confirms the existence of sparsely distributed crystalline nodules in the 17 nm and 34 nm thin samples.

With the observed differences in the evolution of X_c with film thickness in both conditions as displayed in Figure 2**Erreur ! Source du renvoi introuvable.** emerges the question of preferable deposition conditions. As crystalline phase is favorable for electronic transport as well as doping, one could argue the low power conditions are to be favored as they yield a higher doping level and a higher X_c for thick films. However, when looking at thinner films high power conditions will lead to a partially crystalline layer where low power conditions are fully amorphous. Depending on the desired thickness either set of deposition conditions may be prefered. The backside Raman scattering experiment reveals the region close to the substrate stays partially amorphous even with increasing thickness. The extent of that incubation layer is known to be less than the 35 nm necessary to the phase transition in low power conditions (Figure 2 (a)). It must be pointed out that thinner amorphous incubation layers have been obtained for µc-Si:H by using a two step, layer by layer process.[9], [17], [21] However these layers where undoped and as seen in **Erreur ! Source du renvoi introuvable.** (a) the addition of phosphine to the gas mixture prevents crystalline phase nucleation. Thinner incubation layers may also be obtained by further increasing the hydrogen dilution factor R_H, at the cost of a low deposition rate. The importance of the nature of the substrate must also be mentionned as our Raman spectroscopy measurement cannot be conducted for µc-Si:H films deposited on mono-Si. However, similarly to epitaxial growth techniques, the emergence of a crystalline order is favored in presence of an ordered interface. Hence we expect to obtain higher X_c as well as thinner incubation layers for materials deposited on crystalline substrates.

3.2. Electrical properties of P doped µc-Si:H layers

3.2.1. Total and active dopant concentration

Electrical properties of our films were measured using a Hall effect setup and chemical composition in terms of absolute phosphorus concentration in the film was mesured by SIMS in the entire depth of the films and was found to be homogeneously distributed. Results are shown in **Figure 4 (a)**.

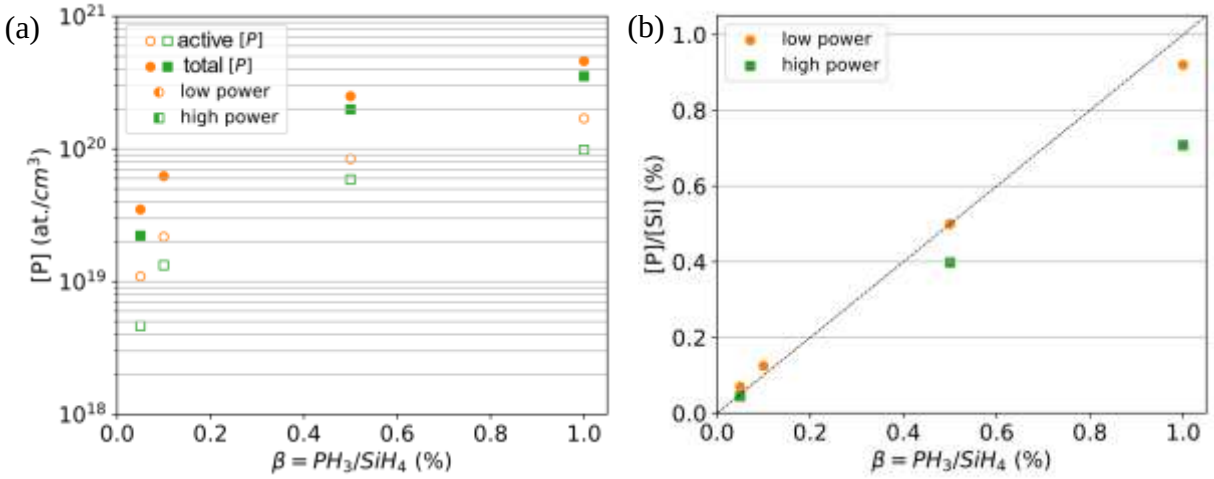

Figure 4: (a) Phosphorus concentration in the deposited films measured by ToF-SIMS , and active P concentration determined by Hall effect, as a function of the phosphine to silane ratio in the PECVD chamber (b) Solid phase phosphorus concentration as a function of gas phase phosphine to silane ratio, the dashed line corresponds to a 1:1 ratio between [P]/[Si] and β

High doping levels are achieved with n > 10^{20} cm^{-3} for the most doped µc-Si:H layers, with a higher [P] for low power samples, regardless of the measurement technique used. In both set of samples and for the whole range of doping investigated the activation rate of incorporated dopant atoms, i.e. the $[P]_{Hall}/[P]_{SIMS}$, is over 30 %. It is encouraging considering that µc-Si:H contains numerous structural defects when compared to its monocrystalline counterpart. At equivalent phosphine level β, our sample exhibit a doping level two orders of magnitude greater than what was reported by Wei et al.[18] while Backhausen et al.[22] have reached similar doping levels with β = 2 %. An excess in defects or segregation of phosphorus to grain boundaries would have led to a lower activation rate and thus made it impossible to reach these high doping levels. The detailed values of conductivity σ, mobility µ and doping levels n obtained by Hall effect measurement are reported in **Erreur ! Source du renvoi introuvable.**. The uncertainty is less than 0.1 % for σ and less than 5% for n and µ. **Figure 4 (b)** reveals almost no preferential incorporation of phosphorus in the film compared to silicon. In the studied range, the [P]/[Si]

ratio is linearly dependant on the dopant gas flow ratio β with a slight preference for P incorporation in low power ($r = [P]/(\beta \cdot [Si]) = 0.94$) over high power ($r = 0.73$) conditions. Such behaviour can be explained in terms of bond dissociation energy of Si-H and P-H bonds, as both values are close yet E_D(P-H) = 3.55 eV > E_D(Si-H) = 3.08 eV.[23]

3.2.2. Limitations of Hall effect measurement

Raman scattering experiments provide a depth-averaged information on X_c. However the thick samples (168 nm and 310 nm, for low and high power deposited films, respectively) used for Hall effect measurements were analysed considering the assumption of a homogeneous and isotropic material. In these layers, the amorphous incubation layer may act as a high resistance in parallel to the low resistance microcrystalline layer. As the calculation for the doping level involve film thickness, an under estimation of the effective doping level, and consequently of the activation rate of the crystalline phase is likely. A rough estimation of the order of magnitude of the error commited on doping level measurement can be performed considering the layer is mainly amorphous for the initial 30 nm deposited (Figure 2**Erreur ! Source du renvoi introuvable.** (a)). The doping level could be underestimated by 18 % and 10 % in low and high power conditions, respectively.

Table 2 : Hall effect measurement of conductivity (σ), mobility (μ) and doping level at room temperature in the Van Der Pauw configuration.

β	*low power*			*high power*		
	σ [S.cm^{-1}]	μ [cm².V^{-1}.s^{-1}]	doping level [cm^{-3}]	σ [S.cm^{-1}]	μ [cm².V^{-1}.s^{-1}]	doping level [cm^{-3}]
0.05%	1.078	0.615	-1.09E+19	0.338	0.454	-4.64E+18
0.10%	2.195	0.630	-2.18E+19	0.812	0.385	-1.33E+19
0.50%	8.772	0.651	-8.41E+19	5.690	0.602	-5.90E+19
1.00%	13.218	0.487	-1.70E+20	9.512	0.602	-9.86E+19

4. Conclusion

PECVD conditions suited for deposition of phosphorus highly doped microcrystalline silicon were found. Tendency of P doped μc-Si:H to undergo a crystalline to amorphous transition was prevented by increasing Hydrogen dilution from R_H = 25 to 50, leading to a decrease in deposition rate. In such conditions, AFM and Raman crystallinity measurements revealed that a high power (100 W) and high pressure (1 Torr) regime leads to a more continuous nucleation of crystallites with film thickness contrary to the low power regine (30 W, 0.8 Torr) which grows as an amorphous layer for the first 23 nm before crystalline phase nucleation. Without a fully

amorphous incubation layer, high power conditions could be better suited for electrical contact layers in PIN junctions. An experimental comparison of the electrical performance of a PIN device with either low or high power n-type layer would be needed in order to confirm our hypothesis. SIMS and Hall effect measurements show that lower power and pressure (30 W, 800 mTorr) conditions leads to a 20% higher phosphorus incorporation in the film from the plasma. However activation rate of incorporated phosphorus does not depend on the deposition conditions chosen and n-type doping levels reaching 1.7×10^{20} cm^{-3} was obtained.

Aknowledgement

This project was funded by STMicroelectronics and CNRS under contract CIFRE N° 2019/1645. The authors would like to thank the Nanolyon platform for their technical support in this project and the CECOMO platform at Institut Lumière et Matière (UMR5306) for the access provided to Raman spectrocopy equipment.

Received: ((will be filled in by the editorial staff))

Revised: ((will be filled in by the editorial staff))

Published online: ((will be filled in by the editorial staff))

References

[1] G. Boucharlat, "Dispositifs à transfert de charges (CCD)," *Électronique*, Aug. 2015, doi: 10.51257/a-v1-e2530.

[2] P. Slangen, N. Long, and P. Picart, "Imagerie numérique ultrarapide," *Mes. Mécaniques Dimens.*, Jun. 2016, doi: 10.51257/a-v1-r6733.

[3] P. De Moor, "3D integration of imagers," presented at the Tipp 2014 - Third International Conference on Technology and Instrumentation in Particle Physics, Effectenbeurszaal, Jun. 03, 2014. Accessed: Dec. 17, 2021. [Online]. Available: https://indico.cern.ch/event/192695/contributions/353250/

[4] N. Moussy *et al.*, "A highly reliable Amorphous Silicon photosensor for above IC CMOS image sensor," in *2006 International Electron Devices Meeting*, Dec. 2006, pp. 1–3. doi: 10.1109/IEDM.2006.346978.

[5] S. D. Brotherton, J. R. Ayres, A. Gill, H. w. van Kesteren, and F. J. a. M. Greidanus, "Deep levels of copper in silicon," *J. Appl. Phys.*, vol. 62, no. 5, pp. 1826–1832, Sep. 1987, doi: 10.1063/1.339564.

[6] A. Dey and D. Das, "Narrow band gap high conducting nc-Si1-xGex:H absorber layers for tandem structure nc-Si solar cells," *J. Alloys Compd.*, vol. 806, pp. 1529–1535, Oct. 2019, doi: 10.1016/j.jallcom.2019.07.320.

[7] T. Matsui, C.-W. Chang, T. Takada, M. Isomura, H. Fujiwara, and M. Kondo, "Micro-crystalline Si1-xGex Solar Cells Exhibiting Enhanced Infrared Response with Reduced

Absorber Thickness," *Appl. Phys. Express*, vol. 1, no. 3, p. 031501, Mar. 2008, doi: 10.1143/APEX.1.031501.

[8] T. Matsui *et al.*, "Application of microcrystalline Si1−xGex infrared absorbers in triple junction solar cells," in *2010 35th IEEE Photovoltaic Specialists Conference*, Jun. 2010, pp. 000311–000316. doi: 10.1109/PVSC.2010.5615904.

[9] P. Roca i Cabarrocas, "Plasma enhanced chemical vapor deposition of amorphous, polymorphous and microcrystalline silicon films," *J. Non-Cryst. Solids*, vol. 266–269, pp. 31–37, May 2000, doi: 10.1016/S0022-3093(99)00714-0.

[10] Q. Guo and X. Geng, "Deposition High Quality P-type Microcrystalline Silicon Thin Films by RF-PECVD," in *2019 6th International Conference on Systems and Informatics (ICSAI)*, Nov. 2019, pp. 263–267. doi: 10.1109/ICSAI48974.2019.9010228.

[11] M. Krause, H. Stiebig, R. Carius, and H. Wagner, "Microcrystalline Germanium Photodetectors," *MRS Proc.*, vol. 664, p. A26.5.1, 2001, doi: 10.1557/PROC-664-A26.5.1.

[12] Z. Li, W. Li, Y. Jiang, H. Cai, Y. Gong, and J. He, "Raman characterization of the structural evolution in amorphous and partially nanocrystalline hydrogenated silicon thin films prepared by PECVD," *J. Raman Spectrosc.*, vol. 42, no. 3, pp. 415–421, 2011, doi: https://doi.org/10.1002/jrs.2711.

[13] S. Veprek, F.-A. Sarott, and Z. Iqbal, "Effect of grain boundaries on the Raman spectra, optical absorption, and elastic light scattering in nanometer-sized crystalline silicon," *Phys. Rev. B*, vol. 36, no. 6, pp. 3344–3350, Aug. 1987, doi: 10.1103/PhysRevB.36.3344.

[14] E. Bustarret, M. A. Hachicha, and M. Brunel, "Experimental determination of the nanocrystalline volume fraction in silicon thin films from Raman spectroscopy," *Appl. Phys. Lett.*, vol. 52, no. 20, pp. 1675–1677, May 1988, doi: 10.1063/1.99054.

[15] D. M. Zhigunov, G. N. Kamaev, P. K. Kashkarov, and V. A. Volodin, "On Raman scattering cross section ratio of crystalline and microcrystalline to amorphous silicon," *Appl. Phys. Lett.*, vol. 113, no. 2, p. 023101, Jul. 2018, doi: 10.1063/1.5037008.

[16] A. Matsuda, "Amorphous and Microcrystalline Silicon," in *Springer Handbook of Electronic and Photonic Materials*, S. Kasap and P. Capper, Eds. Cham: Springer International Publishing, 2017, pp. 573–587. doi: 10.1007/978-3-319-48933-9_25.

[17] S. Hamma, D. Colliquet, and P. R. Cabarrocas, "Microcrystalline Silicon Growth: Deposition Rate Limiting Factors," *MRS Online Proc. Libr. Arch.*, vol. 507, ed 1998, doi: 10.1557/PROC-507-505.

[18] W. Wei, G. Xu, J. Wang, and T. Wang, "Raman spectra of intrinsic and doped hydrogenated nanocrystalline silicon films," *Vacuum*, vol. 81, no. 5, pp. 656–662, Jan. 2007, doi: 10.1016/j.vacuum.2006.09.006.

[19] E. Vallat-Sauvain, U. Kroll, J. Meier, N. Wyrsch, and A. Shah, "Microstructure and surface roughness of microcrystalline silicon prepared by very high frequency-glow discharge using hydrogen dilution," *J. Non-Cryst. Solids*, vol. 266–269, pp. 125–130, May 2000, doi: 10.1016/S0022-3093(99)00769-3.

[20] W. B. Jordan, E. D. Carlson, T. R. Johnson, and S. Wagner, "Structural Evolution of Nanocrystalline Germanium Thin Films with Film Thickness and Substrate Temperature," *MRS Online Proc. Libr.*, vol. 762, no. 1, p. 65, Feb. 2011, doi: 10.1557/PROC-762-A6.5.

[21] K. Saitoh *et al.*, "Role of the hydrogen plasma treatment in layer-by-layer deposition of microcrystalline silicon," *Appl. Phys. Lett.*, vol. 71, no. 23, pp. 3403–3405, Dec. 1997, doi: 10.1063/1.120324.

[22] U. Backhausen, R. Carius, F. Finger, P. Hapke, U. Zastrow, and H. Wagner, "Hall-Effect Studies on Microcrystalline Silicon with Different Structural Composition and Doping," *MRS Online Proc. Libr.*, vol. 452, no. 1, pp. 833–838, Dec. 1996, doi: 10.1557/PROC-452-833.

[23] D. P. Stevenson, “The Strengths of Chemical Bonds,” *J. Am. Chem. Soc.*, vol. 77, no. 8, pp. 2350–2350, Apr. 1955, doi: 10.1021/ja01613a116.